

Anisotropy of exchange stiffness and its effect on the properties of magnets

K. D. Belashchenko

Department of Physics and Astronomy, University of Nebraska, Lincoln, Nebraska 68588

Using the spin-spiral formulation of the tight-binding linear muffin-tin orbital method, the principal components of the exchange stiffness tensor are calculated for typical hard magnets including tetragonal CoPt-type and hexagonal YCo₅ alloys. The exchange stiffness is strongly anisotropic in all studied alloys. This anisotropy makes the domain wall surface tension anisotropic. Competition between this anisotropic surface tension and magnetostatic energy controls the formation and dynamics of nanoscale domain structures in hard magnets. Anisotropic domain wall bending is described in detail from the general point of view and with application to cellular Sm-Co magnets. It is shown that the repulsive cell-boundary pinning mechanism in these magnets is feasible only due to the anisotropic exchange stiffness if suitably oriented initial pinning centers are available. In polytwinned CoPt-type magnets the exchange stiffness anisotropy controls the orientation of macrodomain wall segments. These segments may reorient both statically during microstructural coarsening and dynamically during the macrodomain wall splitting in external field. Reorientation of segments may facilitate their pinning at antiphase boundaries.

I. INTRODUCTION

The formation and dynamics of magnetic domain structures are commonly studied by micromagnetic methods employing the phenomenological gradient expansion for the ‘exchange term’ in the free energy.¹ For a crystal of arbitrary symmetry this term may be generally written as

$$F_{\text{ex}} = A_{\alpha\beta} \int \frac{\partial e_\gamma}{\partial r_\alpha} \frac{\partial e_\gamma}{\partial r_\beta} d^3r \quad (1)$$

where $\mathbf{e}(\mathbf{r}) = \mathbf{M}(\mathbf{r})/M$ is the unit vector parallel to magnetization, summation is assumed over repeated Cartesian indices, $A_{\alpha\beta} = MD_{\alpha\beta}/4$, and $D_{\alpha\beta}$ is the spin-wave stiffness tensor which determines the long-wavelength part of the magnon spectrum as $\hbar\omega(\mathbf{q}) = D_{\alpha\beta}q_\alpha q_\beta$. In a cubic crystal $A_{\alpha\beta} = A\delta_{\alpha\beta}$ where $\delta_{\alpha\beta}$ is the Kronecker symbol, and A is commonly referred to as the exchange constant. Below $A_{\alpha\beta}$ is referred to as the exchange stiffness tensor.

A cubic crystal may only have a fourth-order magnetocrystalline anisotropy (MCA) in the spin-orbit coupling parameter ξ , while a non-cubic crystal has MCA in the second order in ξ . Since magnetic hardness generally requires high MCA, all known hard magnets are non-cubic. Many of them are uniaxial, so that $A_{\alpha\beta}$ has two principal components, in-plane A_{ab} and out-of-plane A_{c} .

The components of the exchange stiffness tensor may be found both theoretically using non-collinear spin-polarized band structure calculations, and experimentally, from the long-wavelength part of the magnon dispersion spectrum. Nevertheless, to my knowledge, none of these methods was applied to hard magnets, and the isotropic model ($A_{\text{c}} = A_{\text{ab}} = A$) was explicitly used in all micromagnetic calculations (see, e.g., Refs. 2,3), while A is usually estimated from the Curie temperature.⁴ This paper reports the results of calculations of A_{ab} and A_{c} for several uniaxial hard magnets including CoPt, FePt, FePd and the SmCo₅-like compound YCo₅. It turns out

that exchange stiffness anisotropy in hard magnets is typically quite large.

Strong anisotropy of exchange stiffness may significantly affect the hysteretic properties of a magnet, because it translates into anisotropic domain wall surface tension:

$$\gamma_n = 4(A_n K)^{1/2} \quad (2)$$

where K is the MCA constant, and A_n is the exchange stiffness along the direction normal to the domain wall. Therefore, the domain walls have a tendency to align normal to the magnetically soft direction (the one with the lowest A_n).

On the other hand, according to the pole avoidance principle, the magnetostatic contribution to the free energy prefers to eliminate the ‘magnetic charges’ $\rho = -\text{div } \mathbf{M}$ localized on the domain walls by aligning them parallel to the magnetization axis. For a magnet with easy-axis MCA, if $A_{\text{ab}} < A_{\text{c}}$ then the exchange term favors the alignment of domain walls parallel to the easy axis, just as the magnetostatic term. However, if $A_{\text{ab}} > A_{\text{c}}$ as in all studied alloys, then the exchange and magnetostatic terms favor different (orthogonal) domain wall orientations. The relative importance of these terms depends on the length scale and geometry of the domain structure. As we will see below, the exchange term often dominates in hard magnets with sufficiently fine domain structures. In this case common considerations based on the pole avoidance principle are inapplicable, and various peculiarities in the domain structure and its response to the external magnetic field should be expected.

The rest of the paper is organized as follows. Anisotropy of exchange stiffness in several typical hard magnets is determined using first-principles calculations in Section II. Temperature dependence of the exchange stiffness anisotropy is discussed in Section III. The following sections describe the effects of exchange stiffness anisotropy on the properties of the domain structure. Anisotropic domain wall bending is considered

in Section IV from the general point of view. The effect of anisotropic domain wall bending on the coercivity of cellular Sm-Co magnets is addressed in Section V. Section VI examines the effects of exchange stiffness anisotropy on the structure of domain walls and coercivity of polytwinned CoPt type magnets. Section VII concludes the paper.

II. CALCULATION OF EXCHANGE STIFFNESS IN CoPt TYPE AND YCo₅ MAGNETS

The values of A_{ab} , A_c were calculated using the spin-spiral formulation⁵ of the tight-binding linear muffin-tin orbital (TB-LMTO) method within the atomic sphere approximation (ASA) including the ‘combined correction’ term.⁶ The spin-spiral (“frozen magnon”) approach is much more reliable compared to the calculation of exchange stiffness based on a finite number of pair exchange parameters, because in practice the corresponding sum in real space does not converge.

Local spin density approximation (LSDA) was used with von Barth-Hedin exchange-correlation potential.⁷ The calculations were done for experimental values^{8,9,10} of lattice constants given in Table I. The atomic sphere radii for both constituents were taken to be equal to each other in CoPt, FePt and FePd. In YCo₅ the radii were 3.548 a.u. for Y and 2.627 a.u. for Co in both inequivalent positions. The calculations were repeated for two setups with three ($l_{\max} = 2$) and four ($l_{\max} = 3$) basis functions per atom, and care was taken to achieve convergence with the Brillouin zone sampling. Spin-orbit coupling was neglected.

In the spin-spiral method the direction of the magnetic moment at site i depends on coordinates as

$$\mathbf{e}_i = (\sin \theta \cos \mathbf{q}\mathbf{r}_i, \sin \theta \sin \mathbf{q}\mathbf{r}_i, \cos \theta) \quad (3)$$

where \mathbf{q} is the wave vector and θ the amplitude of the spin spiral. For a spin spiral with small q at zero temperature, according to (1), we have

$$E/V = A_{\alpha\beta} q_{\alpha} q_{\beta} \sin^2 \theta. \quad (4)$$

where E and V are the excess total energy referenced from the ferromagnetic state and volume of the computational cell.

The results listed in Table I show that the exchange stiffness anisotropy is quite large in all studied alloys. Notably, A_{ab} is everywhere greater than A_c due to the predominantly in-plane bonding between Fe or Co atoms. For comparison, the values of A_{ab} and A_c were also calculated for hcp cobalt. Here the exchange stiffness is almost isotropic as expected, and its value of approximately 3.5×10^{-6} erg/cm (or $D \simeq 600$ meV·Å²) is in good agreement with experiment¹¹ and with other calculations.^{12,13} The exchange stiffness for both directions is larger in YCo₅ compared to CoPt type alloys due to higher Co concentration. A_{ab} in YCo₅ is close to that in hcp Co.

TABLE I: Lattice parameters and calculated values of in-plane and out-of-plane exchange stiffness (units of 10^{-6} erg/cm). The value given before (after) the slash was calculated with $l_{\max} = 2$ ($l_{\max} = 3$).

	CoPt	FePt	FePd	YCo ₅	Co
a , Å	3.806	3.861	3.860	4.937	2.507
c/a	0.968	0.981	0.968	0.806	1.623
A_{ab}	1.70/1.58	1.10/0.87	1.89/1.78	3.97/3.89	3.55
A_c	1.13/1.03	0.38/0.06	0.87/0.72	1.68/1.57	3.43
$\alpha = A_c/A_{ab}$	0.66/0.65	0.34/0.07	0.46/0.40	0.42/0.40	0.97

The out-of-plane exchange stiffness in FePt is unusually small and very sensitive to the lattice parameter c . This magnetostructural effect may be quantified by the value $W = dA_c/d \ln c = 26 \cdot 10^{-6}$ erg/cm. Low value of A_c and high value of W imply that moderate compression of the order of 1–2% along the c axis may induce magnetic instability in FePt with the formation of a spin wave in the c direction. This conclusion agrees qualitatively with the results of other studies suggesting that the layered antiferromagnetically ordered (AFM) state (a special case of such spin wave) in FePt has lower energy compared to the ferromagnetic (FM) state under moderate c/a reduction¹⁴ or even at experimental lattice parameters.¹⁵ However, strong sensitivity of A_c to the basis set (see Table 1) indicates that ASA is too crude for the description of magnetic energetics in FePt. On the other hand, the LSDA approximation also seems to be insufficient, because adding any of the two types of gradient corrections^{16,17} to the LSDA exchange-correlation potential notably tends to stabilize the FM phase.

Competition between different magnetic structures (including non-collinear ones) is characteristic for fcc phases of iron¹⁸ and its alloys (Fe₃Pt is a known Invar alloy), and hence it is not surprising for FePt. Indeed, while FePt is tetragonal, its structure fully retains the topology of the fcc lattice if Fe and Pt sites are considered equivalent.

From the practical point of view, structural sensitivity of A_c in FePt suggests that the exchange stiffness anisotropy in this magnet may be controlled using chemical pressure,¹⁴ appropriate doping or off-stoichiometry. In view of the strong effect of this anisotropy on the hysteretic properties (see below), this possibility may prove useful in applications, such as the design of perpendicular magnetic recording media.

III. TEMPERATURE DEPENDENCE

It is obvious that exchange stiffness anisotropy α is an additional parameter of micromagnetics which may have a strong effect on the coercivity and other properties of magnets. In this connection it is worth noting that in some materials α may strongly depend on temperature and doping. For example, consider a layered magnet with atoms of type A in even layers and type B in odd lay-

ers. Suppose that the exchange interaction is strong for A–A pairs, negligible for B–B pairs, and small for A–B pairs. This is a good approximation for all CoPt type magnets, where A corresponds to the 3d metal, and B to Pt or Pd. If we assume that the magnitudes of the magnetic moments M_A and M_B do not depend on temperature (rigid local moments model), in the mean field approximation the reduced magnetization of the B layer $m_B = \langle \mathbf{M}_B \rangle / M_B$ is

$$m_B = f(2J_{BA}m_A/T) \quad (5)$$

where $m_A = \langle \mathbf{M}_A \rangle / M_A$, $f(x) = \coth(x) - 1/x$, and $J_{BA} = \sum_j J_{ij}$ where site i is within the B layer and j runs over A sites. Since J_{BA} , as we assumed, is much smaller than J_{AA} (defined with both i and j in the A layer), there is a wide range of temperatures where the alloy is still ferromagnetic, but $J_{BA}/T \lesssim 1$. In this region $f(x) \approx x/3$, and, supposing that the Curie temperature T_c is almost entirely determined by A–A interactions ($T_c \approx 2J_{AA}/3$), we obtain

$$\frac{m_B}{m_A} \approx \frac{J_{BA}}{J_{AA}} \frac{T_c}{T}, \quad (6)$$

that is, the ratio of magnetizations of B and A sublattices is inversely proportional to temperature. Obviously, the relative contribution of A–B pairs to A_{ab} and A_c in the mean-field approximation follows the same law. At the same time, due to the layered structure the A–B pairs may give an important contribution to A_c at $T = 0$ (according to the calculation, this is the case in FePt). Eq. (6) implies that close to T_c this contribution is reduced by a factor J_{BA}/J_{AA} , and hence α is essentially determined only by exchange interaction in A–A pairs.

In addition, in magnets like FePt the induced magnetic moments of Pt atoms should be more easily destroyed by thermal excitations compared to the self-induced, well-localized Fe moments, and the temperature dependence of α should be even more pronounced.

On the other hand, non-magnetic impurities in a layered system (e.g. Cu in SmCo₅) may energetically prefer some specific layers. At high concentration of such impurities the interlayer exchange coupling will be strongly reduced, again decreasing α and also enhancing its temperature dependence.

These effects provide an interesting mechanism for the dependence of magnetic properties on temperature and doping due to the increased domain wall bending. This relationship may be important in Sm-Co type magnets where domain walls are heavily bent, as discussed in Section V.

IV. ANISOTROPIC DOMAIN WALL BENDING

Bending of pinned domain walls in external magnetic field was invoked by many authors to describe

certain aspects of coercivity and hysteresis in magnets.^{19,20,21,22,23,24} This bending, which generally manifests itself in the initial magnetic susceptibility, was incorporated in the Globus model to describe the hysteresis loop of granular magnets.²⁰ Pinning of bending domain walls on an array of defects was also considered by a number of authors, see Ref. 22 and references therein.

In real magnets domain wall bending may play a more subtle role in the magnetization reversal. For some microstructures bending of domain walls may facilitate their pinning by increasing the area of contact with pinning centers. In particular, this mechanism was discussed in the studies of coercivity and hysteresis loop in SmCo₅ powders²¹ and in cellular Sm–Co magnets.^{23,24}

In previous treatments of domain wall bending the exchange stiffness was assumed to be isotropic. Here we will discuss the effect of exchange stiffness anisotropy on the domain wall bending.

First, we will study domain wall bending neglecting the associated stray fields. As we will see below, this approximation is valid when the characteristic flux closure length is sufficiently small.

To get a general feeling of the problem of domain wall bending, it is useful to invoke a direct analogy between domain walls and foam bubbles. Indeed, in the presence of external magnetic field \mathbf{H} the domain walls in a uniaxial magnet experience constant pressure of magnitude $2\mathbf{M}\mathbf{H}$ directed away from the regions where $\mathbf{H}\mathbf{M}$ is positive. On the other hand, if the exchange stiffness tensor is isotropic, the free energy of a domain wall is simply proportional to its total area, just as that of a foam membrane.

This analogy allows one to guess the equilibrium configurations of domain walls pinned by certain symmetric pinning sites. For example, a domain wall pinned by a circular defect should obviously have the form of a sphere segment with radius R related to the external field as $R = \gamma(\mathbf{M}\mathbf{H})^{-1}$ (the Laplace pressure $2\gamma/R$ of the curved domain wall compensates the applied pressure $2\mathbf{M}\mathbf{H}$). This result was obtained in Ref. 24 where the sphere segment was used as a variational trial function. A domain wall pinned at two parallel straight lines assumes cylindrical shape with twice as smaller radius; this solution was discussed for a domain wall in a thin ferroelectric film.²⁵

If exchange stiffness is anisotropic, the analogy with the foam membrane no longer holds, because the domain wall surface tension is also anisotropic. Denoting the angle between the normal to the domain wall and the magnetization axis as ϕ , the surface tension of the domain wall is given by (2) with

$$A_n = A_{ab} \sin^2 \phi + A_c \cos^2 \phi \quad (7)$$

Consider a domain wall pinned at a closed curve B with a typical size R_0 lying in the $x = 0$ plane, choosing the z axis parallel to the easy magnetization axis. The shape of the domain wall is defined by a function $\xi = \xi(y, z)$ with $\xi = 0$ at the boundary B . The total free energy is

easily shown to be (we still neglect the stray fields and assume for simplicity that \mathbf{H} is parallel to the z axis):

$$F = \int \left[\gamma_{ab} \sqrt{1 + (\partial_y \xi)^2 + \alpha (\partial_z \xi)^2} - 2MH\xi \right] dydz \quad (8)$$

where γ_{ab} is the surface tension of a domain wall parallel to the z axis, the integral is taken over the area bounded by B , and $\partial_y \equiv \partial/\partial y$, etc. In the isotropic case Eq. (8) reduces to the expressions of Refs. 24,25. In zero field the equilibrium shape of the domain wall is just $\xi = 0$, while at $H \neq 0$ it satisfies the Euler-Lagrange equation corresponding to the variational problem $\delta F = 0$:

$$(\partial_y R^{-1} \partial_y + \alpha \partial_z R^{-1} \partial_z) \xi + R_{ab}^{-1} = 0, \quad (9)$$

where R is the square root from Eq. (8), and $R_{ab}^{-1} = 2MH/\gamma_{ab}$ is the domain wall curvature for “in-plane bending” (i.e. that with $\partial_z \xi \equiv 0$). The role of exchange stiffness anisotropy is seen most clearly for the case when the external field is weak, $H \ll \gamma(MR_0)^{-1}$, and $\xi \ll R_0$. In this case we obtain to first order in ξ :

$$(\partial_y^2 + \alpha \partial_z^2) \xi + R_{ab}^{-1} = 0 \quad (10)$$

Eq. (10) shows that the domain wall bends more easily “out of plane” ($\partial_y \xi = 0$) if $\alpha < 1$ and “in plane” ($\partial_z \xi = 0$) if $\alpha > 1$. Indeed, if the boundary B is formed by two straight segments parallel to the z direction as in Ref. 25 (e.g., pinholes in a film) at distance $L = 2R_0$ from each other, then ξ does not depend on z , and from (10) we obtain the angle of domain wall deflection at the pinning site: $\beta = 2MHR_0/\gamma_{ab}$. On the other hand, if the boundary B is formed by straight lines parallel to y direction (e.g., scratches on a film surface), then ξ does not depend on y , and the deflection angle is α^{-1} times larger. The latter configuration is shown in Fig. 1.

The practical implication of this result is that the efficiency of pinning centers in a magnet with anisotropic exchange stiffness depends on their orientation. In $\alpha < 1$ case typical for hard magnets the domain walls bend more easily when pinned by defects that are normal to the magnetization axis.

The exact shape of the domain wall in external field may be found from the solution of the Euler-Lagrange equation without the assumption $\xi \ll R_0$. This yields the circular cylinder segment²⁵ of radius R_{ab} for in-plane bending, and the elliptic cylinder segment for out-of-plane bending:

$$(\xi - \xi_0)^2 + \alpha^{-1} z^2 = R_{ab}^2 \quad (11)$$

where $\xi_0^2 = R_{ab}^2 - R_0^2/\alpha$.

Now, let us clarify the role of magnetostatic (stray) fields. If the domain wall is parallel to the magnetization axis z , it has no net magnetic charge. Any deviation from this alignment produces magnetic charge on the wall with surface density $\sigma = 2M \cos \phi$, where ϕ is defined exactly as in Eq. (7). Obviously, in-plane domain wall bending does not induce any charges on the wall, and we should

only be concerned about stray fields when we are dealing with out-of-plane curvature.

To estimate when stray fields may notably affect out-of-plane domain wall bending, we have to compare the magnetostatic energy $\delta\epsilon_m$ generated by domain wall charging to the excess surface free energy $\delta\epsilon_s$ associated with this bending (both energies are defined per unit length in the y direction). We assume that the domain wall is pinned by two line defects parallel to the y axis and displaced from each other by a distance $L = 2R_0$ along the z axis, as shown in Fig. 1. We will find $\delta\epsilon_m$ and $\delta\epsilon_s$ for a domain wall bent in a weak field. As follows from Eq. (10), in this case the domain wall is shaped as a segment of a circular cylinder of large radius $R = \alpha R_{ab}$. Substituting this solution in Eq. (8) we obtain $\delta\epsilon_s \approx \frac{1}{3} \alpha \gamma_{ab} R_0^3 / R^2$.

The magnetostatic energy is given by the integral

$$\delta\epsilon_m = -\frac{1}{2} \int \mathbf{M} \mathbf{H}_m dx dz \quad (12)$$

where \mathbf{H}_m is the stray field generated by the surface charges on the domain wall. The distribution of these charges is antisymmetric with respect to the $z = 0$ plane (see Fig. 1), and the stray field obviously falls off at the length scale of R_0 . The total positive charge per unit length of the wall is of the order $\rho_+ \approx MR_0^2/R$ (assuming $R \gg R_0$). Since the magnetization is reversed at the domain wall, there is a strong cancellation in the integral (12). Indeed, using the superposition principle, let us add a fictitious domain wall which is a mirror image of the real domain wall with respect to the $x = 0$ plane. This fictitious wall is shown in Fig. 1 by the gray dashed line. Mirror reflection also reverses the sign of the magnetic charges. For symmetry considerations, the contribution to the integral (12) from *outside* of the lens-shaped area between the real and fictitious walls doubles when the fictitious charges are added. At the same time, this contribution is negligibly small, because the two walls form a thin capacitor, and the field is confined to its interior. Therefore, only this interior region of cross-section $\frac{4}{3}R_0^3/R$ contributes to $\delta\epsilon_m$. The stray field in this area is of the order $2\rho_+/R_0$ (now we should take the field only from the real domain wall), and from (12) we find $\delta\epsilon_m \approx \frac{4}{3}M^2R_0^4/R^2$. Thus, we obtain $\delta\epsilon_m/\delta\epsilon_s = \nu M^2R_0/(\alpha\gamma_{ab})$ where the form-factor $\nu \approx 4$. This relation also holds when the curvature is not small ($R \sim R_0$), but ν should be somewhat different.

The relative importance of the magnetostatic energy increases linearly with R_0 . Using the relation $\gamma_{ab} = 4K\delta_{ab}/\pi$ where $\delta_{ab} = \pi(A_{ab}/K)^{1/2}$ is the in-plane domain wall width, we find that $\delta\epsilon_m$ overcomes $\delta\epsilon_s$ at $L \sim l_{cr} = 4\alpha\delta_{ab}/\eta$, where $\eta = 2\pi M^2/K$ is the dimensionless magnetostatic parameter (in hard magnets η is small, e.g. in $\text{Sm}_2\text{Co}_{17}$, CoPt and FePt it is close to 0.1). Thus, at $L \lesssim l_{cr}$ the external field works mainly against the domain wall surface tension, and its anisotropy is reflected in the domain wall bending according to Eq. (9). At $L \gtrsim l_{cr}$ the external field works mainly against magneto-

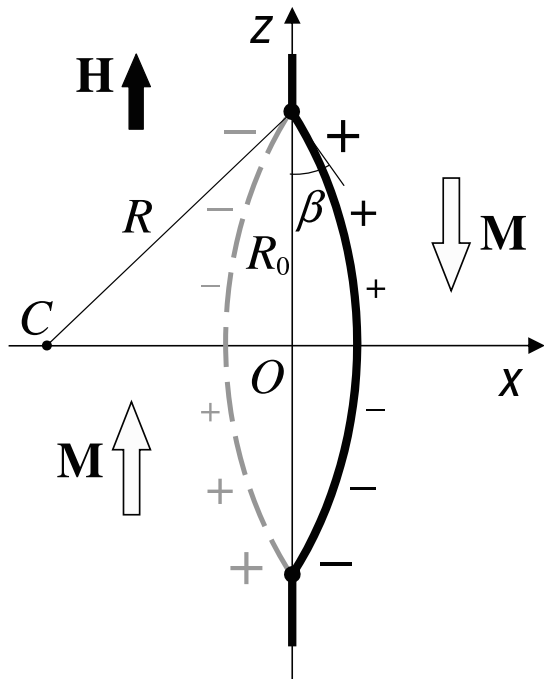


FIG. 1: Cylindrical out-of-plane bending of a domain wall (thick solid line) pinned by two line defects located at $x = 0$, $z = \pm R_0$. C is the axis, and R the radius of the cylindrical domain wall. β is the domain wall deflection angle at the defect. The gray dashed line shows the fictitious domain wall used in the calculation of the magnetostatic energy. The size of plus and minus symbols schematically shows the magnetic charge density on the real and fictitious walls.

static forces, which makes the contribution of surface tension (together with its anisotropy) unimportant. By minimizing the total free energy given by Eq. (8) with $\delta\epsilon_m$ added, we find the deflection angle taking into account all energy terms: $\beta \simeq \beta_0 L / (l_{cr} + L)$ where $\beta_0 = H/2M$. Note, however, that this expression is approximate, because the equilibrium shape of the domain wall at $L \gtrsim l_{cr}$ is no more a cylindrical segment, and because we derived it assuming $R \gg R_0$. At $L \ll l_{cr}$ this result coincides with β found above neglecting the stray fields. However, as L is increased beyond l_{cr} , β approaches its asymptotic limit β_0 and stops changing.

In general, the parameter l_{cr} appears in all problems when magnetostatic interaction competes with the domain wall energy. In a specific geometry, the characteristic *flux closure length* l_f should be compared with this parameter. At $l_f \gg l_{cr}$ the magnetostatic interaction dominates; at $l_f \ll l_{cr}$ it may be neglected. In particular, the crossover length l_{cr} has the order of the material parameter λ of the magnetic bubble domain theory (see, e.g., Ref. 26). Together with η , this parameter also controls the structure of charged domain walls in thin films.²⁷ The critical single-domain size of a particle R_{sd} is also proportional to l_{cr} ; for example, for a sphere with isotropic exchange stiffness $R_{sd} \approx 5.6\delta/\eta$.⁴

V. CELLULAR Sm-Co MAGNETS

Magnetization reversal in cellular Sm-Co magnets involves heavy bending of domain walls. Since the anisotropy of exchange stiffness strongly affects the ability of domain walls to bend, it is likely to play an important role in the development of coercivity. In this section we will focus on the model of repulsive domain wall pinning at the cell boundaries and show that this mechanism can not be realized unless the exchange stiffness is strongly anisotropic, and specifically oriented line defects (such as those provided by the platelet phase) are available for domain wall pinning *in addition* to the cell boundaries.

Precipitation-hardened magnets based on an appropriately doped $\text{Sm}_2\text{Co}_{17}$ - SmCo_5 system develop outstanding magnetic hardness in a wide range of temperatures. It is associated with the formation of a cellular microstructure where rhomboid $\text{Sm}_2\text{Co}_{17}$ -based (2:17) cells are surrounded by SmCo_5 -based (1:5) boundary phase^{28,29,30} and is usually explained by domain wall pinning at the cell boundaries.²⁸ Some other mechanisms of coercivity were also suggested.^{31,32,33}

Whether pinning at the cell boundaries is attractive or repulsive depends on the magnetic properties of 2:17 and 1:5 phases for the given (doped) system. Recent experiments of Kronmüller and Goll³⁴ support the hypothesis that pinning is repulsive at room temperature but attractive at high temperatures, which also explains the anomalous temperature dependence of coercivity (see Ref. 31 and references therein).

The estimated unpinning field for the cell boundaries (in the *plane-parallel* configuration) agrees with the experimentally observed coercivity.³⁴ However, this does not fully explain high coercivity, because magnetization reversal always takes the path of lowest energetic barriers. It is not sufficient for a high barrier to be present; it is necessary that there be no way around it. The domain walls might move parallel to the hexagonal axis and never align parallel to the cell boundaries. In order to be pressed against the cell boundaries, the domain walls must bend in the external field. Skomski²⁴ estimated the deflection angle β of a domain wall at a pinning site at 56° assuming $H = 0.8$ T, cell size $L = 80$ nm, spherical bending, and isotropic exchange stiffness.

However, this value of the external field appears to be too high for this estimate. Indeed, domain wall bending requires pinning at some ‘seed defects’ other than the cell boundaries.³⁵ In order to estimate the unpinning field for these defects, we note that the coercivity of samples that had not been subjected to slow cooling is only of the order of 0.1 T.³⁴ The role of slow cooling is likely to promote the formation of the 1:5 phase with segregated copper.³⁴ Assuming that the properties of the 2:17 cells are essentially unchanged during the slow cooling, we may take the value of 0.1 T as an estimate of the unpinning field for the seed defects. The same value corresponds to domain wall pinning at the vertices of the cells.²⁴ Thus, we

obtain $\beta \approx 6^\circ$ which is clearly insufficient to press the domain wall against the cell boundary.

The above estimate assumes spherical bending and isotropic exchange stiffness. In reality, it is reasonable to assume that the values of exchange stiffness anisotropy in the 2:17 phases of the Sm-Co and Y-Co systems are very close because exchange coupling is dominated by Co-Co pairs. Indeed, the Curie temperatures of all R_2Co_{17} phases (where R is a rare-earth atom or yttrium) are almost identical,⁴ while the 2:17 phase may be obtained from the 1:5 phase simply by a replacement of every third samarium atom by a Co_2 dumbbell. Thus, we assume that the factor α in pure Sm_2Co_{17} is close to its value of 0.4 obtained for YCo_5 at $T = 0$ (Table 1). How does this affect the estimate of β ? As follows from Eq. (10), exchange stiffness anisotropy strongly facilitates domain wall bending only if it is pinned by line defects normal to the magnetization axis (as in Fig. 1). In this case the deflection angle β contains an additional factor of α^{-1} due to exchange stiffness anisotropy and a factor of 2 due to the fact that bending is cylindric instead of spheric. This brings β to 30° , neglecting the effect of stray fields.

The magnetostatic term in the total energy of a bent domain wall is notable, although not yet dominating for the cell size $L = 80$ nm. Indeed, taking $A_{ab} = 4 \times 10^{-6}$ erg/cm and $\alpha = 0.4$ as found above for YCo_5 , $K = 3 \times 10^7$ erg/cm³ (Ref. 34), and $M = 950$ emu/cm³ we obtain $\gamma_{ab} = 44$ erg/cm², $\delta_{ab} = 12$ nm, $\eta = 0.15$, and $l_{cr} \approx 130$ nm. Using the approximate formula from Section IV, we arrive at the final estimate of $\beta \approx 18^\circ$.

Let us summarize the results obtained above. For the typical cell size of 80 nm the external field of 0.1 T (corresponding to the unpinning of uncurved walls) may induce the domain wall deflection of about 18° if the exchange stiffness anisotropy is large and if the domain walls may be initially pinned by line defects normal to the magnetization axis. If either of these two conditions is not met, the domain walls only deflect by about 6° before they are unpinned from the initial pinning centers.

According to these estimates, the deflection angle does not reach the typical cell-boundary inclination of 30° . Although our assumptions may be loosened up to some extent (for example, allowing for a somewhat larger unpinning field for uncurved walls), it seems clear that the repulsive cell-boundary pinning mechanism of coercivity may only be realized in Sm-Co magnets under a very favorable set of circumstances. In particular, it requires the presence of initial pinning defects normal to the z axis.

High coercivity develops in Sm-Co magnets *only* when they are doped with zirconium³⁶ which promotes the formation of thin lamellae normal to the hexagonal axis of the crystal. The intersections of these lamellae with cell boundaries have the “right” orientation needed for high coercivity in the repulsive pinning case. Therefore, *if* high coercivity of cellular Sm-Co magnets is due to repulsive pinning at the cell boundaries, it is likely that the lamellar phase provides the initial pinning centers

for domain wall bending. This conclusion does not contradict the observation³⁴ that in the low-coercivity state obtained after annealing at 800°C the microstructure and the platelet phase are fully developed. Indeed, the platelet phase simply provides initial pinning sites which may be useful only in the presence of strongly pinning cell boundaries developing only after the slow cooling. However, the microscopic origin of pinning at the initial pinning sites is yet to be determined.

VI. SLANTING AND ‘SMART PINNING’ OF DOMAIN WALLS IN CoPt-TYPE MAGNETS

In this section we will explore the effects of exchange stiffness anisotropy on the structure of domain walls and magnetization reversal in polytwinned CoPt-type magnets. The microstructure of these magnets consists of regular stacks of L1₀-ordered domains (c -domains). In each stack the c -domains are separated by parallel twin boundaries in one of the $\{110\}$ planes.^{37,38,39,40,41} There is always a high density of antiphase boundaries within the c -domains.^{37,38,39,40,42}

Usually the c -domain thickness d is large compared to the domain wall width $\delta \sim 5$ nm, and each c -domain may be regarded as an individual magnetic domain with intrinsic 90° domain walls at the twin boundaries.⁴¹ The dynamic domain structure is formed by macrodomain walls^{40,41} crossing many twin boundaries in a stack. These walls are split at the twin boundaries, and their segments are coupled only by relatively weak magnetostatic forces.⁴³

Below we study the effects of exchange stiffness anisotropy on the properties of macrodomain walls. We will describe the orientation of macrodomain wall segments, the energetical preference of different global macrodomain wall orientations, the rotation of segments during macrodomain wall splitting in external field, and the relation of these properties with coercivity.

Consider a $(1\bar{1}0)$ oriented macrodomain wall shown schematically in Fig. 2. As it is shown by large empty arrows, the magnetization in each c -domain is parallel to the easy c axis, and it is reversed at the macrodomain wall. The exchange stiffness A_n is given by Eq. (7) where ϕ , as shown in Fig. 2, is now the angle between the normal to the domain wall segment and the tetragonal axis c . Without magnetostatic interaction, the surface tension of the macrodomain wall (e.g., the free energy of the domain wall segment per unit normal cross-section) is $4(A_n K)^{1/2} [\cos(\frac{\pi}{4} - \phi)]^{-1}$. Minimizing over ϕ we obtain

$$\tan \phi = \alpha \quad (13)$$

where, as above, $\alpha = A_c/A_{ab}$. This result is analogous to a similar expression obtained for an antiphase boundary.⁴⁴ We see that for $A_c = A_{ab}$ (isotropic exchange stiffness) $\phi = \pi/4$ as it should be — the domain wall has no preferential orientation and simply minimizes its area by aligning perpendicular to the twin boundaries. For

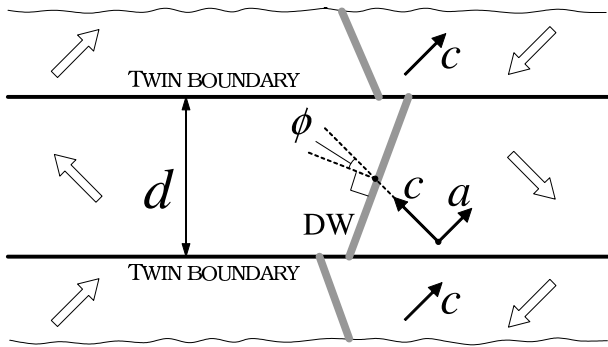


FIG. 2: Macrodomain wall in the polytwinning stack (three c -domains shown). The central segment of the wall is marked DW. Large empty arrows show the of magnetization. Arrows marked ‘ c ’ show the tetragonal axes in each c -domain; arrow marked ‘ a ’ shows one of the other two four-fold axes of the parent fcc lattice. If x and y coordinates are assigned to a and c axes of the central c -domain, the macrodomain wall has a global $(1\bar{1}0)$ orientation.

$A_c \neq A_{ab}$ the domain wall segments slant so as to decrease the surface tension.

Segments of a $(1\bar{1}0)$ macrodomain wall carry magnetic charges of alternating signs,⁴³ and the flux closure length l_f is obviously of the order of the c -domain thickness d . Therefore, at $d \gtrsim l_{cr}$ the magnetostatic interaction dominates, and the segments align parallel to the tetragonal axis to get rid of the magnetic charge, while at $d \ll l_{cr}$ their orientation is determined by Eq. (13). Here l_{cr} is proportional to δ/η , but the form-factor is different from that found in Section IV for domain wall bending. In CoPt and FePt l_{cr} is of the order of 50 nm. Thus, while d increases during the microstructural coarsening, the domain wall segments gradually slant from the angle given by (13) towards the tetragonal axis.⁴⁵

Contrary to the $(1\bar{1}0)$ oriented macrodomain wall, the segments of a (001) oriented one are perpendicular to the twin boundaries at any d , because this minimizes both the surface energy and the magnetostatic energy. At $d \gtrsim l_{cr}$ the (001) macrodomain wall has lower energy than the $(1\bar{1}0)$ one because its segments do not carry any magnetic charge. However, at $d \ll l_{cr}$ the preferential global orientation is determined by exchange stiffness anisotropy. The surface tension for (001) and $(1\bar{1}0)$ macrodomain walls (per unit normal cross-section) is γ_{ab} and $\gamma_{ab} [2\alpha/(1+\alpha)]^{1/2}$, respectively. Therefore, at $\alpha > 1$ the (001) orientation is favorable, while in the typical case $\alpha < 1$ the $(1\bar{1}0)$ orientation is favorable. This explains why macrodomain walls observed in FePt crystals have $\{110\}$ orientation⁴¹ while those in FePd with much larger η and hence smaller l_{cr} have $\{100\}$ orientation.⁴⁶

High coercivity of CoPt-type magnets is likely due to the combination of macrodomain wall splitting and pinning of their segments at antiphase boundaries.^{47,48} The highest possible coercivity is achieved when antiphase boundaries are planar, and domain wall segments are parallel to them.⁴⁹ The antiphase boundaries in CoPt-type

magnets often have a preferential crystallographic orientation, which is clear from theoretical considerations,⁴⁴ and observed experimentally for CoPt.³⁹ Typically they slant towards the tetragonal axis, *contrary* to the domain wall segments which slant away from the tetragonal axis at $A_c < A_{ab}$ and $d \ll l_{cr}$. This means that while d increases during the microstructural coarsening, at some point the domain wall segments will become parallel to the preferential orientation of antiphase boundaries producing a maximum in the coercivity.

Interestingly, a similar segment rotation may occur dynamically. If the external field above the splitting threshold⁴⁷ is applied parallel to the twin boundaries, the macrodomain wall is split in two “partial macrodomain walls” which are driven apart from each other. One partial wall is composed of segments in all odd c -domains, and the other of segments in even c -domains. Suppose that $d \ll l_{cr}$ so that the orientation of segments in the $(1\bar{1}0)$ macrodomain wall is given by Eq. (13). Since these segments carry magnetic charges of $\pm 2M \cos \phi$ per unit area, the two partial macrodomain walls carry equal charge densities of opposite sign. The corresponding stray field makes an additional contribution ΔE to the magnetostatic energy proportional to the distance L between the partial macrodomain walls. If the angle ϕ were fixed, at $L \gtrsim l_{cr}$ this positive contribution would dominate over the surface energy of the segments (now the flux closure length l_f is clearly L). Therefore, as the two partial macrodomain walls move apart (L is increased to l_{cr}), their segments gradually rotate toward the tetragonal axis to get rid of the magnetic charge.

As a result, at some L the segments of a splitting macrodomain wall become parallel to antiphase boundaries, just as in the case of increasing d discussed above. If the typical distance between antiphase boundaries is smaller than l_{cr} (the scale of L where domain wall segment rotation occurs), the segments will be pinned by antiphase boundaries at the plain-parallel configuration. In this scenario the coercivity achieves its highest possible value for suitably oriented polytwinning stacks at any $d \ll l_{cr}$, i.e. at relatively early stages of coarsening. This mechanism may play an important role in real CoPt-type magnets developing high coercivity just at these early stages.

VII. CONCLUSION

Using the spin-spiral version of the TB-LMTO method, the in-plane and out-of-plane principal components of the exchange stiffness tensor were calculated for several typical hard magnets. The results show that this tensor usually has a considerable anisotropy. The out-of-plane component is smaller than the in-plane one in all studied hard magnets except pure hcp Co where exchange stiffness is isotropic. The anisotropy is especially high in FePt. In certain materials with intrinsically non-magnetic layers (CoPt, FePt, etc.) the anisotropy of exchange stiffness

may strongly increase at finite temperatures or with suitable non-magnetic doping.

Anisotropy of exchange stiffness may have a strong effect on the orientation of domain walls and on their resistance to bending, and hence on the hysteretic properties of the magnet. These effects may be expected whenever the typical flux closure length associated with the stray fields does not exceed the crossover length $l_{cr} \propto \delta/\eta$ (see Section IV).

Low out-of-plane exchange stiffness facilitates out-of-plane domain wall bending. This effect is crucial for the development of coercivity in cellular Sm-Co magnets in the repulsive cell-boundary pinning regime. This regime may be realized only in the presence of linear pinning defects normal to the magnetization axis (such as the intersections of lamellae with the cell boundaries) providing initial pinning centers necessary for the domain walls to bend and get pressed against the strongly pinning cell boundaries. However, the estimates obtained in Section V suggest that the set of conditions for the realization of this regime is very strict.

In polytwinned CoPt-type magnets the competition between the anisotropy of exchange stiffness and magnetostatic interaction controls the orientation of domain wall segments and the preferential global macrodomain wall orientation. In particular, the domain wall segments gradually rotate toward the tetragonal axis during the microstructural coarsening as the *c*-domains become

thicker. If the antiphase boundaries have a preferential orientation, the coercivity achieves its maximum at the *c*-domain thickness when the domain wall segments become parallel to the antiphase boundaries. The same competition also leads to the dynamic rotation of the segments of a macrodomain wall which is being split by the external field. This rotation may result in a dynamic self-locking of domain wall segments at antiphase boundaries.

The effects discussed in this paper demonstrate that the competition between exchange stiffness anisotropy and magnetostatic energy is a crucial driving force behind the formation and dynamics of nanoscale domain structures in hard magnets.

Acknowledgments

I am much indebted to V.P. Antropov for numerous useful discussions and suggestions, and to M. van Schilfgaarde for the use of his computer codes. I also thank R. Sabirianov and R. Skomski for useful discussions. A large part of this work was carried out at Ames Laboratory, which is operated for the U.S. Department of Energy by Iowa State University under Contract No. W-7405-82. This work was supported by the Director for Energy Research, Office of Basic Energy Sciences of the U.S. Department of Energy.

-
- ¹ C. Kittel, *Quantum theory of Solids* (Wiley, New York, 1963).
 - ² H. Kronmüller, R. Fischer, M. Seeger and A. Zern, *J. Phys. D: Appl. Phys.* **29**, 2274 (1996).
 - ³ J. Fidler and T. Schrefl, *J. Phys. D: Appl. Phys.* **33**, R135 (2000).
 - ⁴ R. Skomski and J.M.D. Coey, *Permanent magnetism* (IOP Publishing, Bristol, 1999).
 - ⁵ V.P. Antropov, M.I. Katsnelson, B.N. Harmon, M. van Schilfgaarde and D. Kusnezov, *Phys. Rev. B* **54**, 1019 (1996).
 - ⁶ O.K. Andersen, *Phys. Rev. B* **12**, 3060 (1975).
 - ⁷ U. von Barth and L. Hedin, *J. Phys. C* **5**, 1629 (1972).
 - ⁸ W. Grange, I. Galanakis, M. Alouani, M. Maret, J.-P. Kappler and A. Rogalev, *Phys. Rev. B* **62**, 1157 (2000).
 - ⁹ P. Villars and L.D. Calvet, *Pearson's handbook of crystallographic data for intermetallic phases* (American Society for Metals, Metals Park, OH, 1985).
 - ¹⁰ C. Chacon, O. Isnard, *J. Phys. Condens. Matter* **13**, 5841 (2001).
 - ¹¹ M.B. Stearns, in: *Landolt-Börnstein Numerical Data*, New Series, Group III, vol. 19, subvol. a, ed. H.P.J. Wijn (Springer, Berlin, 1986), p. 24.
 - ¹² J.M. Bass, J.A. Blackman and J.F. Cooke, *Phys. Rev. B* **53**, 2556 (1996).
 - ¹³ X. Liu, M.M. Steiner, R. Sooryakumar, G.A. Prinz, R.F.C. Farrow and G. Harp, *Phys. Rev. B* **53**, 12166 (1996).
 - ¹⁴ H. Zeng, R. Sabirianov, O. Mryasov, M.L. Yan, K. Cho and D.J. Sellmyer, *Phys. Rev. B* **66**, 184425 (2002).
 - ¹⁵ G. Brown, T.C. Schulthess, A. Janotti, G.M. Stocks, B. Kraccek and D.D. Johnson, *Bull. Amer. Phys. Soc.* **48**, 398 (2003).
 - ¹⁶ D.C. Langreth and M.J. Mehl, *Phys. Rev. Lett.* **47**, 446 (1981); *Phys. Rev. B* **28**, 1809 (1983); C.D. Hu and D.C. Langreth, *Phys. Scr.* **32**, 391 (1985).
 - ¹⁷ J.P. Perdew, in *Electronic Structure of Solids '91*, edited by P. Ziesche and H. Eschrig (Akademie Verlag, Berlin, 1991), p. 11; J. P. Perdew and Y. Wang, *Phys. Rev. B* **45**, 13244 (1992).
 - ¹⁸ E. Sjöstedt and L. Nordström, *Phys. Rev. B* **66**, 014447 (2002), and references therein.
 - ¹⁹ M. Kersten, *Z. Angew. Phys.* **8**, 313 (1956).
 - ²⁰ A. Globus, *C. R. Acad. Sci.* **255**, 1709 (1962); A. Globus and P. Duplex, *IEEE Trans. Magn.* **MAG-2**, 441 (1966); M.A. Escobar, R. Valenzuela and L.F. Magaña, *J. Appl. Phys.* **54**, 5935 (1983).
 - ²¹ H. Zijlstra, *J. Appl. Phys.* **41**, 4881 (1970).
 - ²² H.R. Hilzinger and H. Kronmüller, *J. Magn. Magn. Mater.* **2**, 11 (1976).
 - ²³ K.-D. Durst, H. Kronmüller and W. Ervens, *Phys. Stat. Sol. A* **108**, 705 (1988).
 - ²⁴ R. Skomski, *J. Appl. Phys.* **81**, 5627 (1997).
 - ²⁵ T.J. Yang, V. Gopalan, P.J. Swart and U. Mohideen, *Phys. Rev. Lett.* **82**, 4106 (1999).
 - ²⁶ A.H. Bobeck and E. Della Torre, *Magnetic bubbles* (Amsterdam, North Holland, 1975).
 - ²⁷ A. Hubert, *IEEE Trans. Magn.* **MAG-15**, 1251 (1979).
 - ²⁸ J.D. Livingston and D.L. Martin, *J. Appl. Phys.* **48**, 1350

- (1977).
- ²⁹ J. Fidler and P. Skalicky, J. Magn. Magn. Mater. **27**, 127 (1982).
 - ³⁰ W. Tang, Y. Zhang, A.M. Gabay, H. Kronmüller and G.C. Hadjipanayis, in: Proceedings of the 17th International Workshop on Rare-Earth Magnets and Their Applications, ed. G.C. Hadjipanayis and M.J. Bonder (Rinton Press, Newark, Delaware, 2002), p. 685.
 - ³¹ W. Tang, Y. Zhang, A.M. Gabay and G.C. Hadjipanayis, J. Magn. Magn. Mater. **242-245**, 1335 (2002).
 - ³² B.Y. Wong, M. Willard and D.E. Laughlin, J. Magn. Magn. Mater. **169**, 178 (1997).
 - ³³ M. Katter, J. Weber, W. Assmus, P. Schrey and W. Rodewald, IEEE Trans. Magn. **32**, 4815 (1996); M. Katter, J. Appl. Phys. **83**, 6721 (1998).
 - ³⁴ H. Kronmüller and D. Goll, Scr. Mater. **47**, 545 (2002); Physica B **319**, 122 (2002); Scr. Mater. **48**, 833 (2003).
 - ³⁵ A similar concept was used by Durst *et al.*²³ to explain the inflections of the initial magnetization curve assuming attractive cell boundary pinning in the same group of magnets.
 - ³⁶ W. Tang, Y. Zhang and G.C. Hadjipanayis, J. Appl. Phys. **87**, 5308 (2000).
 - ³⁷ L.-Q. Chen, Y. Wang and A.G. Khachaturyan, Phil. Mag. Lett. **65**, 15 (1992).
 - ³⁸ K.D. Belashchenko, I.R. Pankratov, G.D. Samolyuk and V.G. Vaks, J. Phys.: Condens. Matter **14**, 565 (2002).
 - ³⁹ C. Leroux, A. Loiseau, D. Broddin and G. van Tendeloo, Phil. Mag. B **64**, 58 (1991).
 - ⁴⁰ C. Yanar, J.M.K. Wiezorek and W.A. Soffa, in *Phase Transformations and Evolution in Materials*, ed. P. Turchi and A. Gonis (TMS, Warrendale, 2000), p. 39.
 - ⁴¹ N.I. Vlasova, G.S. Kandaurova and N.N. Shchegoleva, J. Magn. Magn. Mater. **222**, 138 (2000).
 - ⁴² Ya.S. Shur, L.M. Magat, G.V. Ivanova, A.I. Mitsek, A.S. Yermolenko and O.A. Ivanov, Phys. Met. Metallogr. **26**, 241 (1968).
 - ⁴³ K.D. Belashchenko and V.P. Antropov, J. Appl. Phys. **91**, 8474 (2002).
 - ⁴⁴ V.G. Vaks, JETP Lett. **73**, 237 (2001).
 - ⁴⁵ Simultaneously the magnetic structure of each domain wall segment transforms from Bloch-type to Néel-type in the center of the *c*-domain, while it remains Bloch-type in the vicinity of the twin boundary. The configuration of the domain wall segments at the initial stage of this transition for *d* ~ 20 nm was shown in Fig. 1 of Ref. 43.
 - ⁴⁶ B. Zhang and W.A. Soffa, Phys. Stat. Sol. A **131**, 707 (1992).
 - ⁴⁷ K.D. Belashchenko and V.P. Antropov, Phys. Rev. B **66**, 144402 (2002).
 - ⁴⁸ K.D. Belashchenko and V.P. Antropov, J. Magn. Magn. Mater. **253**, 87 (2002).
 - ⁴⁹ A.I. Mitsek and S.S. Semyannikov, Sov. Phys.-Solid State **11**, 899 (1969); R. Friedberg and D.I. Paul, Phys. Rev. Lett. **34**, 1234 (1975); H.R. Hilzinger, Appl. Phys. **12**, 253 (1977); H. Kronmüller, J. Magn. Magn. Mater. **7**, 341 (1978).